Received 7 March 2024; revised 8 May 2024; accepted 26 May 2024. Date of publication 31 May 2024; date of current version 6 August 2024.

Digital Object Identifier 10.1109/OJAP.2024.3406950

Gain Enhancement and Sidelobe Level Reduction of Microstrip Patch Antenna Under Operation of TM_{50}-Like Mode

RENAN A. SANTOS [1], HELTON S. BERNARDO [2], DANILO H. SPADOTI [3], GUILHERME S. DA ROSA [2] (Senior Member, IEEE), AND RAFAEL A. PENCHEL [2] (Member, IEEE)

[1]Faculty of Electrical Engineering, Federal University of Uberlândia (UFU), Uberlândia 38408-100, Brazil

[2]School of Engineering, São Paulo State University (Unesp), São João da Boa Vista 13876-750, Brazil

[3]Institute of Systems Engineering and Information Technology, Federal University of Itajubá (UNIFEI), Itajubá 37500-903, Brazil

CORRESPONDING AUTHOR: R. A. PENCHEL (e-mail: rafael.penchel@unesp.br)

This work was supported in part by the Brazilian Agencies Fundação de Amparo à Pesquisa do Estado de São Paulo (FAPESP) under Grant 2020/09889-4; in part by the Conselho Nacional de Desenvolvimento Cientifico e Tecnológico (CNPq) under Grant 409146/2021-8; in part by the Fundação Coordenação de Aperfeiçoamento de Pessoal de Nível Superior (CAPES)—Finance Code 001 under Grant 88887.885627/2023-00 and Grant 88887.953339/2024-00; in part by the Fundação de Amparo à Pesquisa do Estado de Minas Gerais (FAPEMIG) under Grant APQ-02616-22; and in part by the Agency Financiadora de Estudos e Projetos (FINEP) under Grant 0527/18.

ABSTRACT In this paper, we propose a microstrip patch antenna (MPA) operating in the TM_{50}-like mode, designed for gain enhanced and sidelobe levels (SLLs) reduction. Our methodology involves altering the resonator's surface current distribution by introducing three groups of transverse slots at points of null electric field. Additionally, two symmetrically positioned stubs are utilized to the antenna's gain enhanced. We verify that proper combinations of such artifacts on the proposed radiators significantly reduce the SLL while maintaining the high-gain characteristics of the TM_{50}-like mode. A prototype was fabricated and characterized for operation around 7.6 GHz, in the C band. The results demonstrate that a realized gain of 15.0 dBi can be achieved, with the SLL reduced to approximately 15 dB, representing an excellent option for high-gain applications requiring a low profile and compact size.

INDEX TERMS High-gain, microstrip patch antenna, sidelobe reduction, loading stubs, TM_{50}-like mode.

I. INTRODUCTION

HIGH-GAIN antennas have garnered significant interest due to the rapid advancement in wireless communications, spurred notably by the exponential increase in mobile data traffic associated with fifth and sixth-generation (5G and 6G) networks, and beyond [1]. They enhance the signal-to-noise ratio (SNR), ensuring elevated levels of communication quality [2].

Numerous antenna types exhibit high-gain characteristics, including reflector antennas [3], antenna arrays [4], and lens antennas [5]. However, these structures are typically electrically large, posing limitations for certain applications. In contrast, higher order mode rectangular microstrip patch antennas (MPAs) offer a compelling alternative due to their low profile, compact size, and cost-effectiveness [6].

Typically, ordinary microstrip patch antennas do not achieve high-gain values, exhibiting a directivity of about 7 dBi [7] when operating in the fundamental mode (TM_{01} or TM_{10}). In such scenarios, the radiation characteristics of the MPA can be effectively likened to that of an array of two radiating slots separated by approximately a guided half-wavelength ($\lambda_g/2$). Consequently, the effective radiating area of the antenna is smaller than a quarter-wavelength square (i.e., $\lambda_g/2 \times \lambda_g/2$). To achieve high gain, the metallization of the MPA must be larger relative to the wavelength. Therefore, an alternative is to operate in a higher order mode [8], where the resonator's electrical length is significantly larger than in its fundamental mode, thereby enhancing the antenna (potential) gain [9]. This approach has an advantage over patch antenna arrays in that it eliminates the need for power

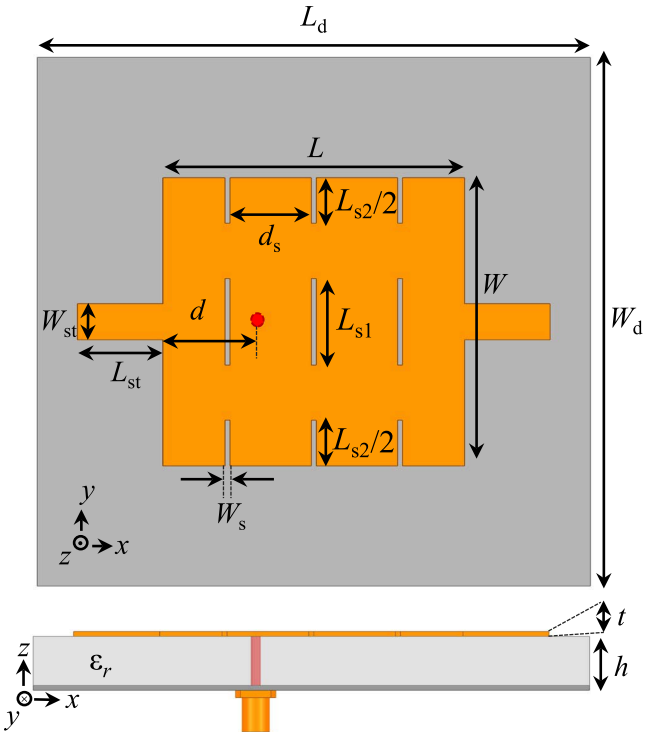

FIGURE 1. The geometry of a MPA operating in the TM_{50}-like mode investigated in the study.

dividers, which reduces losses and leads to more compact devices. However, operating in higher order modes often results in undesired high sidelobe level lobes (SLL), quite similar to an array antenna's grating lobes [7], [10].

Increased sidelobes in an MPA operating in TM_{m0} higher-order modes are primarily due to the enlarged electrical length L of the patch (see Fig. 1 for reference). Indeed, the behavior approximately resembles that of an array of radiating slots spaced by the distance $L \approx m\lambda_g/2$. When operating under the fundamental mode (TM_{10}), $L < \lambda_g/2$ and less than one period of the array factor (AF) appears in the visible region [10, Ch. 8]. For $L > \lambda_g/2$, more than one period will be visible, and there may be more than one major lobe in the visible region, depending on the equivalent element's resultant phasing. For $L > \lambda_g$, two periods will be visible, and a second major lobe (grating lobe) arises with the same intensity as the main one. For the TM_{30} mode, three periods will be visible, and there may be two grating lobes in addition to the main one. Accordingly, for operation under the TM_{50} mode, there may be five high-intensity lobes [10, Ch. 8].

The literature highlights significant contributions towards achieving reduced sidelobes and enhanced gain in MPAs. In [8], two high-directivity MPAs operating in the modified TM_{30} and TM_{50} modes are introduced. They demonstrate broadside radiation patterns with directivities of 15 dBi and 18 dBi, respectively. To accomplish this, the geometries of the antennas are altered by incorporating large slots — two for the TM_{30} mode model and four for the TM_{50} mode model. In [9], a MPA operating under a modified TM_{30} mode is detailed. The research presents the antenna exhibiting a broadside radiation pattern, achieving a gain of 12.7 dBi. This significant performance enhancement was obtained via strategic positioned transverse narrow slots along the patch's central axis.

A dual-polarized MPA operating in a modified TM_{50} mode was presented [11]. The study details the antenna's broadside radiation pattern achieving a gain of 10.9 dBi. The design strategy involved incorporating a single-dielectric layer alongside a straightforward feeding mechanism. This configuration is further enhanced by the inclusion of four identical narrow slots positioned on the cross-shaped radiating patch to optimize performance. In [12], a study was presented on a wideband and gain-enhanced, single-layer, differential-fed rectangular MPA operating in dual radiative TM_{30} and TM_{50} modes. The study unveiled broadside radiation patterns with a gain of 10.7 dBi. To attain these results, the geometry of the antenna was modified by symmetrically etching a pair of long and narrow slots at specific positions on the upper microstrip patch. These positions were strategically chosen where the electric field of the TM_{30} mode peaks, while the electric field of the TM_{50} mode reaches a null point. In [13], a study was introduced that details the design of a dual-polarized 36-element ($3 \times 6 \times 2$) magnetic current array antenna, which is designed without the need for a complex feeding network. Instead, a straightforward approach utilizing a pair of differential feeds is employed to excite the dual-polarized array, maintaining a low profile. This simplified feeding mechanism is facilitated by leveraging the TM_{90} mode of an MPA, complemented by 3×4 identical half-wavelength slots for each polarization to enhance performance. This study reported an antenna gain of 15.7 dBi. In [14], a dual-polarized high-order-mode MPA operating under the dual radiating TM_{03} and TM_{05} modes was proposed to enhance gain and bandwidth using characteristic mode analysis. The antenna presents a broadside radiation with a gain of 9.6 dBi. To achieve this, the antenna's geometry is modified by etching long and narrow slots along the central line of the patch and using vias to shift the TM_{05} mode closer to the TM_{03} mode.

In [15], a novel technique for miniaturization and enhancement of bandwidth and gain in a MPA operating at a TM_{03}-like mode was introduced. Broadside radiation with a gain of 10.5 dBi are presented. To achieve this, the antenna's geometry was modified by placing a wide slot on the patch to reduce sidelobes in the radiation pattern. Additionally, three meandered line linkages are inserted inside the slot to miniaturize the structure while maintaining current continuity.

In [16], a dual-band high-gain MPA operating at modes TM_{10} and TM_{02} was presented. Broadside radiation with gains of 8.65 dBi and 9.12 dBi are reported. The proposed antenna comprises five low-cost FR-4 dielectric substrate layers and ten metal layers with embedded air cavities. The driven patch generates the TM_{10} and TM_{02} modes, while additional modes are generated by etching a U-slot and

horizontal slot on the driven patch to achieve dual-band operation. The stacked patch with the U-slot suppresses the radiation pattern split of the TM_{02} mode, improving the antenna gain in the high-frequency band, and generating radiation null to increase the out-of-band gain-suppression level.

In [17], a method for reducing SLL, improving return loss, and enhancing bandwidth in notch-loaded TM_{30} mode MPAs was presented. Broadside radiation with a gain of 13 dBi are demonstrated. To achieve these improvements, a fractal slot was used in the center of the notch-loaded patch to eliminate unwanted out-of-phase current regions. The study shows that the combination of the fractal slot and notch loading technique can significantly enhance the SLL, return loss, and bandwidth of notch-loaded TM_{30} mode without compromising the gain or symmetry of the radiation patterns.

In [18], a dual-band MPA array with orthogonal circular polarization in two frequency bands, operating at modes TM_{01}/TM_{10} and TM_{03}/TM_{30}, was presented. Broadside radiation with gains of 10.8 dBi and 12.5 dBi are reported. To achieve this, a novel antenna element for such an array is introduced, utilizing symmetrically loaded stubs on the edges of a square patch. This approach modifies the field distribution of TM_{30} to resemble that of TM_{10} — thereby reducing the corresponding electrical length of the patch and avoiding sidelobes.

In this paper, a high-gain MPA design operating under the TM_{50}-like mode is proposed. The design approach combines techniques presented in [9] and [12]. Additionally, two symmetrically positioned stubs at the edges of the patch are utilized to the antenna's gain enhanced, resulting in the antenna geometry depicted in Fig. 1. This approach allows us to reduce the SLLs while maintaining enhanced gain characteristics. The simulated and measured results demonstrate high-gain performance of up to 15.0 dBi, with the SLL reduced to approximately 15 dB when compared with ordinary designs.

The remainder of this paper is organized as follows. Section II introduces the basic antenna configurations under study and the principles of operation theories, focusing on approximate MPA analysis through the cavity method. Section III outlines the antenna design process utilizing the FEM approach provided by commercial software, along with fabrication details. Moreover, Section IV presents both simulation and measured results to assess the impedance bandwidth and radiation performance of the antenna being studied. It also includes a comparative analysis of several antenna performance metrics from recently reported MPAs operating at higher-order modes, emphasizing the advancements of the current design. Finally, in Section V, we present concluding remarks.

II. WORKING PRINCIPLE

A. ANTENNA CONFIGURATION

The radiation characteristics of MPAs can be approximately modelled using the cavity model [7]. Accordingly, the antenna can be represented as a resonant cavity with four slots: two parallel slots at the patch ends with length L, and two other slots at the ends with width W. The radiation can be emitted by the combination of a) two slots at the L ends, b) the two slots at the W ends, or c) by all four slots depending on the mode of operation. Thus, the radiation pattern behaviour is contingent on the operating modes excited in the MPA. In our designs, the excitation probes come from below the materialization patch, as depicted in Fig. 1.

B. OPERATING PRINCIPLE

The patch antennas we are investigating are constructed in a substrate of the thickness (h) witch is generally much smaller than the patch sides L and W, as shown in Fig. 2. In view of that, the normalized electric field of a TM_{mn} mode in a MPA, in a simplified way, can be expressed as [7]

$$E_{mn} \sim \cos\left(\frac{m\pi x}{L}\right)\cos\left(\frac{n\pi y}{W}\right) \tag{1}$$

where m and n represent, respectively, the number of half-cycle field variations along the x and y directions.

For the y-invariant modes, i.e., modes with $n = 0$, the radiation pattern is generated solely by the two radiating slots at the ends of length L. Examples include the fundamental TM_{10}-like mode, as well as the TM_{30}-like and TM_{50}-like modes. A simplified depiction of these modes is provided in Fig. 2, where the labels "1" and "2" denote the slots on sides L.

By analysing MPAs operating under the TM_{m0} mode by the cavity method, the resonant frequency are given by [19]:

$$f_{rm0} \approx \frac{3\times 10^8}{2\sqrt{\epsilon_{\text{ref}}}}\frac{m}{(L+2\Delta L)} \tag{2}$$

where,

$$\epsilon_{\text{ref}} = \left(\frac{\epsilon_r+1}{2}\right) + \left(\frac{\epsilon_r-1}{2}\right)\left(1+\frac{12h}{W}\right)^{-1/2}, \tag{3}$$

$$\frac{\Delta L}{h} = 0.412\frac{(\epsilon_{\text{ref}}+0.3)\left(0.264+\frac{W}{h}\right)}{(\epsilon_{\text{ref}}-0.258)\left(0.8+\frac{W}{h}\right)}. \tag{4}$$

In MPAs operating under the TM_{10} mode, as depicted in Fig. 2(a), the electric field distribution within the dielectric substrate can be mathematically described by a cosine function with the argument $\pi x/L$ in the x-direction. The simulated electric field within the dielectric substrate at zx-plane is represented in Fig. 3(a). Furthermore, the field remains constant in the y-direction, assuming the fringing effect around the patch's four sides is negligible — a common assumption in the cavity model. Under these conditions, the surface current density on the patch can be expressed as a sine function with the argument $\pi x/L$ [9]. Consequently, two radiating slots located at the ends of L are spaced approximately $\lambda_g/2$ apart, generating a broadside radiation pattern perpendicular to the patch and

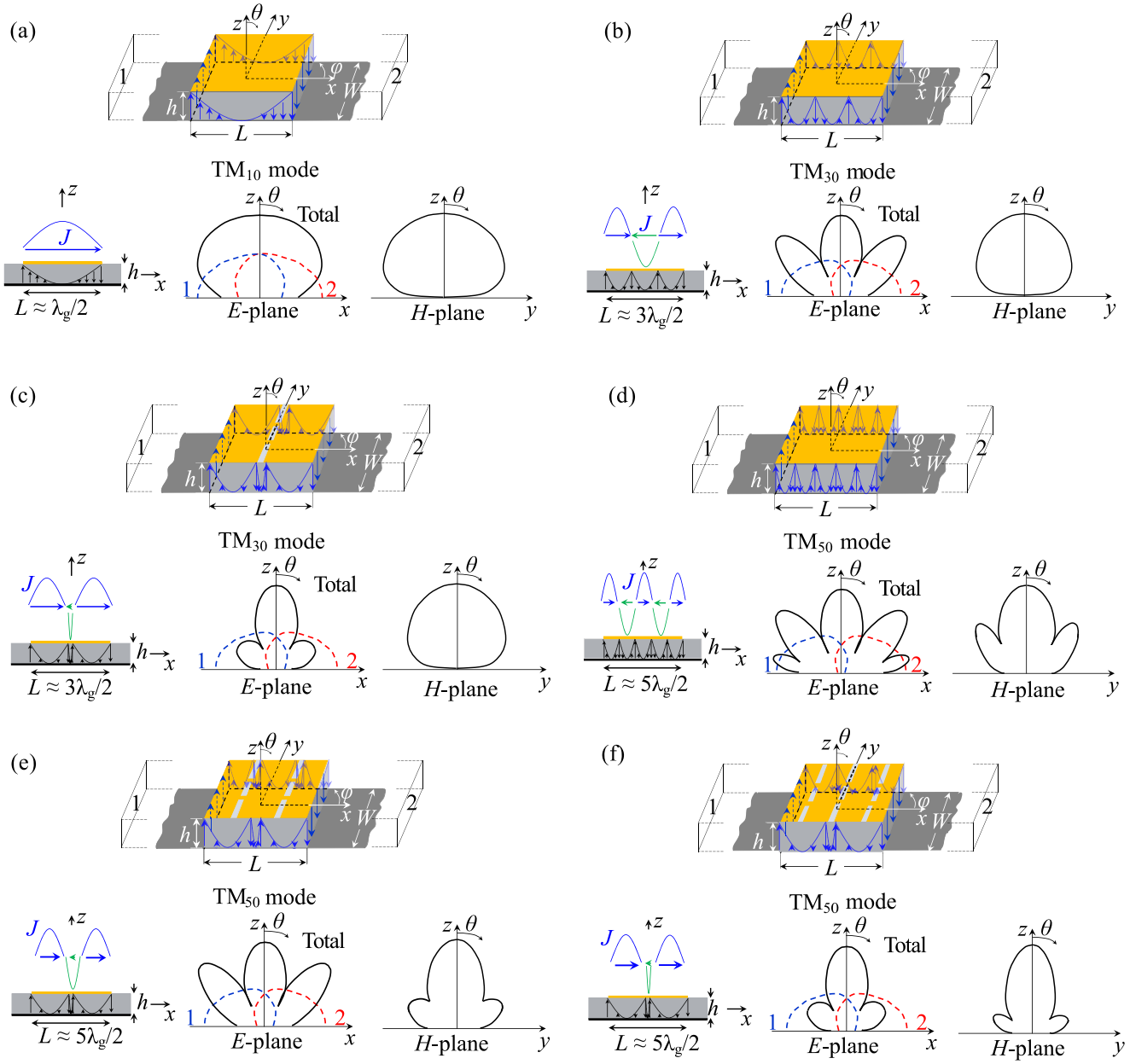

FIGURE 2. Representation of the surface current distribution, field distributions inside the dielectric substrate, and the radiation patterns of the several MPAs operating under high-order modes. (a) Excitation of the TM_{10} mode without slots. (b) Excitation of the TM_{30} mode without slots. (c) Excitation of the TM_{30}-like mode with a transverse slot along the central line in the *x*-direction. (d) Excitation of the TM_{50} mode without slots. (e) Excitation of the TM_{50}-like mode with a pair transverse slot symmetrically etched on specific positions in the *x*-direction. (f) Excitation of the TM_{50}-like mode with a transverse slot along the central line in the *x*-direction and with a pair transverse slot symmetrically etched on specific positions in the *x*-direction.

ground plane. The normalized radiation pattern for each slot in the principal *E*-plane is illustrated individually, along with the combined pattern of the two slots in Fig. 2(a). This configuration does not exhibit sidelobes in *E*- and *H*-planes.

In case of a MPAs operating under the TM_{30} mode, as illustrated in Fig. 2(b), the electric field distribution within the dielectric substrate can be mathematically described by a cosine function with the argument $3\pi x/L$ in the *x*-direction (see Fig. 3(b)). Again, the field remains constant in the *y*-direction. Accordingly, the surface current density on the patch can be expressed as a sine function with the argument $3\pi x/L$ [9]. Consequently, two radiating slots located at the ends of L are spaced approximately $3\lambda_g/2$ apart, creating a broadside radiation pattern perpendicular to the patch and ground plane, accompanied by two relatively pronounced sidelobes in the *E*-plane. This phenomenon, akin to an antenna array, occurs because the radiation from the two slots does not combine perfectly. In the *H*-plane, where field variation tends to be absent, the normalized pattern for each

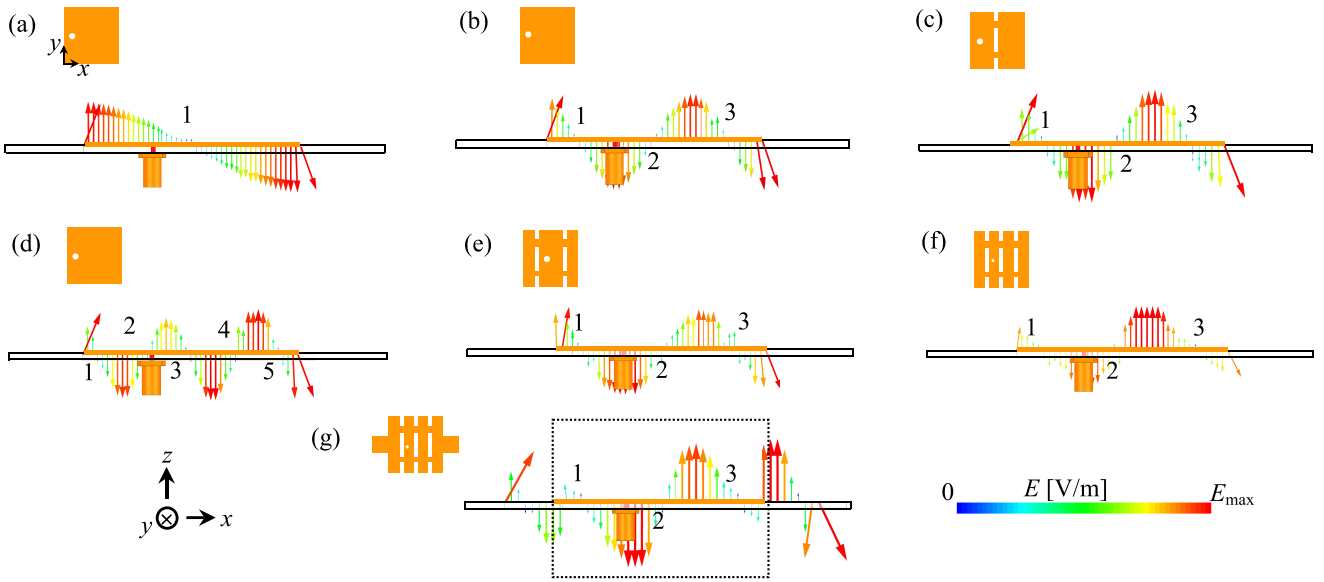

FIGURE 3. Electric distribution on conventional MPA for (a) TM_{10} mode; (b) TM_{30} mode; (c) TM_{30}-like mode with central slots; (d) TM_{50} mode; (e) TM_{50}-like mode with two sets of slots; (f) TM_{50}-like mode with three sets of slots; and (g) TM_{50}-like mode with three set of slots and stubs.

slot and for both combined remains the same, and does not exhibit secondary lobes.

The radiation pattern of the TM_{30} mode can be less desirable due to high SLL values. However, strategies exist for sidelobe reduction and gain enhancement. As detailed in [9], etching a narrow slot along the central line in the x-direction of the patch can alter current flow. This modification forces the out-of-phase current to circulate around it, as depicted in Fig. 2(c). The close proximity of these divided currents results in their far-field radiation nearly cancelling each other out, leading to minimal radiation. Consequently, this technique significantly reduces the SLL in the E-plane by rerouting the out-of-phase current. The resulting field distribution in the dielectric substrate mimics the radiation from an array of two separate radiating slots λ_g apart (Fig. 3(c)) but with a geometric size of $3\lambda_g/2$, achieving a directivity typically exceeding 13 dBi and reducing the SLL to about -20 dB compared to the conventional TM_{30}-like patch shown in Fig. 2(b), i.e., without the slot. It's noteworthy that etching the narrow slot alters the resonant frequency, lowering it. Specifically, in the antenna presented in [9], the frequency shifted from 4.86 GHz without a slot to 4.2 GHz with the inclusion of a narrow slot. It is important to emphasise that these changes in resonance frequencies are not accurately predicted by the cavity method and the formulas presented in Section II-B. As such, these formulas should be considered as a reference or starting point for input into a full-wave electromagnetic solver.

By exploring higher-order modes, in MPAs operating under the TM_{50} mode, as illustrated in Fig. 2(d), the electric field distribution within the dielectric substrate (see Fig. 3(d)) can be mathematically modelled as a cosine function with the argument $5\pi x/L$ in the x-direction according to the cavity model approximations. Similar to the TM_{10} and TM_{30} modes, the surface current density on the patch can be expressed as a sine function with the argument $5\pi x/L$. Consequently, two radiating slots located at the ends of L are spaced approximately $5\lambda_g/2$ apart, generating a broadside radiation pattern perpendicular to the patch and ground plane, accompanied by four pronounced sidelobes in the E-plane. Analogous to an antenna array, this effect arises because the radiation from the two slots does not combine seamlessly. As presented in [10], at the H-plane, there are side lobes, but much smaller than those of the E-plane.

The radiation pattern of the TM_{50} mode can also be less desirable due to high SLL levels. Nonetheless, literature reports strategies for sidelobe reduction and gain enhancement. As documented in [11], [12], and [20] etching two narrow symmetrical slots in specific locations along the x-direction of the patch can redirect the out-of-phase current responsible for the TM_{50}-like mode's external sidelobes, as depicted in Fig. 2(e). The simulated electric field within the dielectric substrate at zx-plane is represented in Fig. 3(e) This adjustment yields a radiation pattern in the E-plane akin to that of a TM_{30}-like mode but with lower SLLs. In [11], the achieved directivity exceeded 10.9 dBi with the SLL reduced to about -12 dB. In [12], a similar design resulted in a directivity exceeding 10 dBi with the SLL reduced to around -20 dB. As mentioned earlier, etching slots into the patch alters the resonant frequency, lowering it. Specifically, in the case reported in [11], the frequency shifted from 7.81 GHz to 5.96 GHz, and in the antenna analyzed in [12], the frequency moved from 8.85 GHz to 5.65 GHz.

Now, etching a narrow slot along the central line in the x-direction of the antenna depicted in Fig. 2(f) can direct the out-of-phase current to flow around it. The proximity of

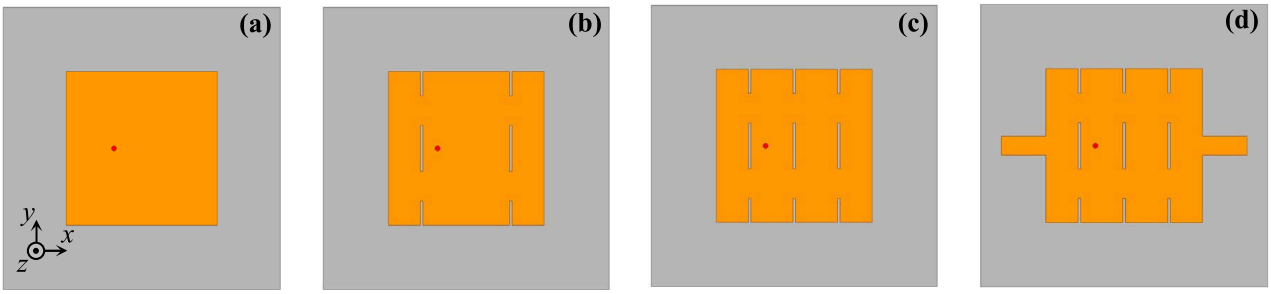

FIGURE 4. Design evolution of the proposed microstrip patch antenna. (a) Conventional MPA operating in the TM_{50}-like mode. (b) MPA operating in the TM_{50}-like mode with two set of slots. (c) MPA operating in the TM_{50}-like mode with three set of slots. (d) MPA operating in the TM_{50}-like mode with three set of slots and with additional stubs.

TABLE 1. The dimensions of the proposed antenna.

Description	Dimensions [in millimeters]										
Models	L	W	L_d	W_d	d	W_s	L_{s1}	L_{s2}	d_s	L_{st}	W_{st}
Conventional	60	60	110	110	19	-	-	-	-	-	-
Two set of slots	60	60	110	110	19	1	18	19	17.5	-	-
Three set of slots	60	60	110	110	19	1	18	19	17.5	-	-
Slots and stubs	60	60	110	110	19	1	18	19	17.5	17	7.5

these bifurcated currents allows for their far-field emissions to nearly negate each other. Consequently, this modification can significantly lower the SLL in the E-plane by rerouting the out-of-phase current. The simulated electric field within the dielectric substrate is represented in Fig. 3(f). Note that we have two TM_{10}-like distribution, each in half the patch (similar to Fig. 2(c)) combining in phase to produce the broadside radiation pattern. The resulting field distribution mimics the radiation from an array of two separate radiating slots λ_g apart but with a geometric size of $5\lambda_g/2$.

III. ANTENNA DESIGN AND ANALYSIS

Fig. 1 illustrates the configuration of the proposed MPA that operates in the TM_{50}-like mode. The antenna's design employs RT/duroid 5880 as the dielectric substrate, characterized by a relative permittivity of 2.20 ± 0.02, a loss tangent of 0.0009, and a thickness of 1.575 mm. The simulations presented in this paper were conducted using the finite element method (FEM) solver provided by ANSYS HFSS [21]. In alignment with the discussions in Section II, it is posited that the antenna's gain enhancement and SLL reduction are principally achieved through the incorporation of slots and stubs into the patch. Consequently, this section delineates the sequential steps undertaken to develop the final antenna model.

Fig. 4 presents the design evolution of the proposed TM_{m0}-like MPA, encompassing the four principal steps of our analysis and design guidance, with the dimensions of each stage detailed in Table 1. The primary dimensions of the antenna remain constant throughout each step, maintaining a square patch configuration with dimensions $L = 60$ mm and $W = 60$ mm. Variations in design are attributed exclusively to the introduction of slots and stubs, as listed in Table 1. In light of the various influencing factors and the lack of precise equations for MPAs operating in high-order modes with slots and stubs, accurate prediction of the resonance frequency and achieving optimal impedance matching demands numerical simulations for precise fine adjustments, with cavity-model-based formulas serving as an initial guide in the design process.

Initially, as depicted in Fig. 4(a), we consider a conventional square MPA designed to operate in the TM_{50}-like mode at a resonance frequency of 8.11 GHz. This operational mode is verified by analyzing the electric field intensity distribution within the dielectric, as illustrated in Fig. 3(d), where five zero points in the electric field are observed along the length L. It is noted that the feed point introduces asymmetries in the E-plane, which become more pronounced in the radiated field. The corresponding radiation patterns are depicted in Fig. 5.

Subsequently, as shown in Fig. 4(b), the antenna was modified with the addition of two sets of symmetrical slots etched onto the patch. This modification yields an electric field distribution akin to that of a TM_{30}-like mode. It is crucial to note that two of the zero points in the electric field along the L-side coincide with the locations of the etched slots, altering the field distribution. Similar to the observations in [12], a shift in the operating frequency to 7.60 GHz was observed. In the E-plane radiation pattern illustrated in Fig. 5(a) we can see a reduction from five to three lobes and in H-plane (see Fig. 5(b)) sidelobe level reduction.

Following this, the antenna is further modified by adding a third set of symmetrical slots, as per the theory primarily outlined in [9], as shown by Fig. 4(c). Now, the field distribution mimics an array of two TM_{10}-like mode patch, as illustrated in Fig. 3(f). This modification, according to [9], alters the field distributions such that the antenna behaves as though it has an electrical length of $5\lambda_g/2$, also resulting in a frequency shift to 7.50 GHz. E-plane (Fig. 5(a)) and H-plane (Fig. 5(b)) radiation patterns shows a significant reduction of the lateral lobes.

Lastly, the proposed MPA with three sets of slots, complemented by stubs, is examined as shown by Fig. 4(d).

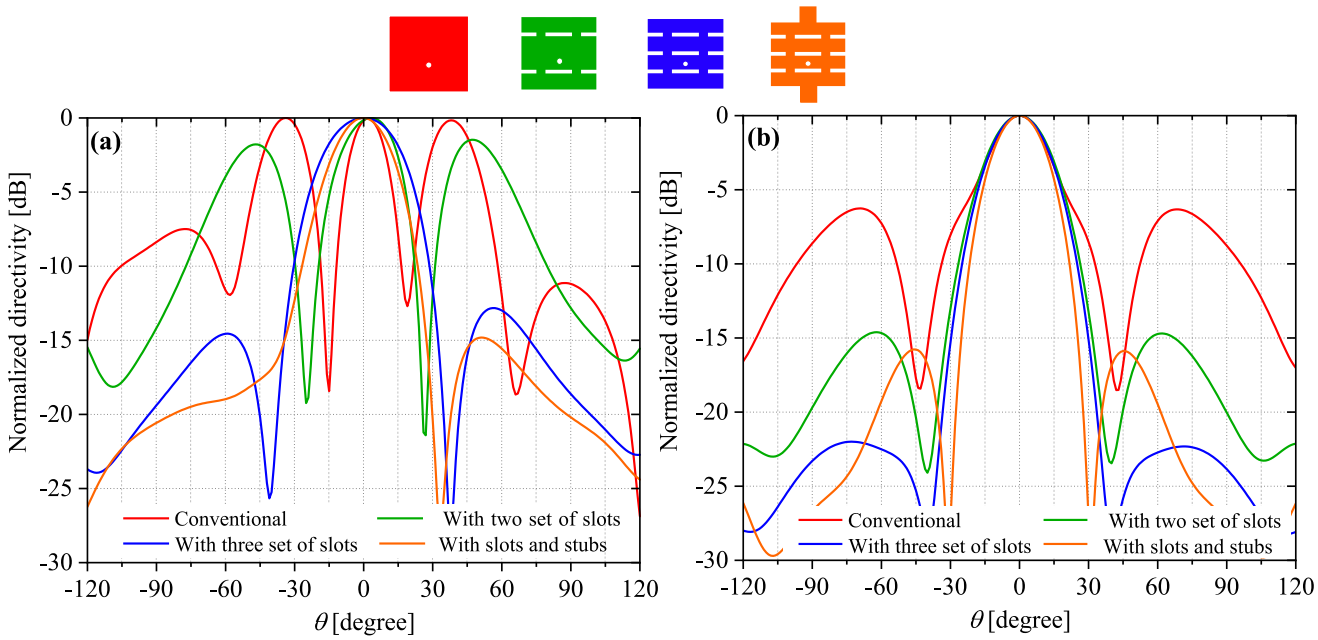

FIGURE 5. Directivity radiation patterns of the four configurations of MPAs operating in the TM_{50}-like mode, as shown in Fig. 4, simulated at their respective resonance frequency. (a) *E*-plane. (b) *H*-plane.

TABLE 2. Performance comparison of the simulated MPAs.

Models	D	$(f_r)_{50}$	λ_0	A_{eff}	A_{g}	ε_{ap}	SLL (E-plane)	SLL (H-plane)
Conventional	7.57	8.11	0.0370	$0.45\lambda_0^2$	$0.327\lambda_0^2$	5	0.0	6.30
With two set of slots	11.82	7.60	0.0410	$1.21\lambda_0^2$	$0.295\lambda_0^2$	15	1.80	14.60
With three set of slots	14.55	7.50	0.0406	$2.27\lambda_0^2$	$0.298\lambda_0^2$	31	14.55	22.00
With slots and stubs	15.37	7.54	0.0398	$2.74\lambda_0^2$	$0.304\lambda_0^2$	35	19.00	15.80

Value of resonance frequency $(f_r)_{50}$ in GHz; Directivity (D) in dBi; aperture efficiency (ε_{ap}) in percentage %; effective area (A_{eff}) in λ_0^2; geometric area of the grounded surface (A_g) in λ_0^2; wavelength at free-space (λ_0) in meter and sidelobe levels (SLL) in dB.

The addition of stubs modifies the field distribution (see Fig. 3(g)) to increase the effective area of the antenna (consequently the directivity and gain) without changing the resonant frequency (see Fig. 6). In this way, it is possible to enhance the electrical length improving SLL of the *E*-plane (Fig. 5(a)) decreasing the SLL in *H*-plane (Fig. 5(b)).

Fig. 7 shows the maximum of directivity (at broadside direction) for the evaluated MPAs. Table 2 provides a comparative analysis of the simulated MPAs' performance. It is noted that the maximum directivity (at broadside direction) at each stage varies, aligning with the respective operating frequencies of the TM_{50}-like mode. Consequently, the directivity observed escalates from 7.57 dBi in the initial MPA design to 15.37 dBi in the final configuration. We verified that using an enlarged patch length of $L + 2L_{\text{st}}$, instead of a stub geometry, significantly reduces the maximum realized gain compared to the stub approach. Consequently, an enlarged patch is discouraged.

Table 2 also compares the resonance frequency, the associated free-space wavelength (λ_0), the effective area (A_{eff}), the geometric area (A_{g}), the aperture efficiency (ε_{ap}), and SLL. The computation of A_g is considered ground area ($A_g = L_d \times W_d$). According to the definitions in [7], we compute:

$$A_{\text{eff}} = \frac{\lambda_0^2 D}{4\pi}, \tag{5}$$

$$\varepsilon_{ap} = \frac{A_{\text{eff}}}{A_g}. \tag{6}$$

To facilitate comparison, the values of A_{g} and A_{eff} are presented as a function of λ_0 for each case, in Table 2. Despite the variations in operating frequency, which result from the introduction of slots and stubs, each incremental modification illustrated in Fig. 4 contributes to an increase in the simulated directivity. This enhancement is accompanied by a corresponding increase in the aperture efficiency, ε_{ap}, which reaches up to 35% in the proposed MPA operating in the TM_{50}-like mode with the incorporation of both slots and stubs.

Fig. 5 presents the comparison of the simulated directivity radiation patterns for the four MPAs under study, on the principal planes, and at their respective operating frequencies.

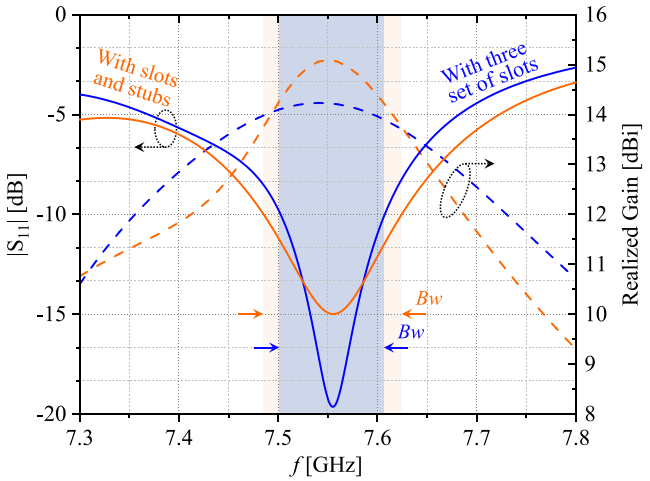

FIGURE 6. Reflection coefficient and realized gain as a function of the frequency for the proposed MPAs with three set of slots with and without stubs.

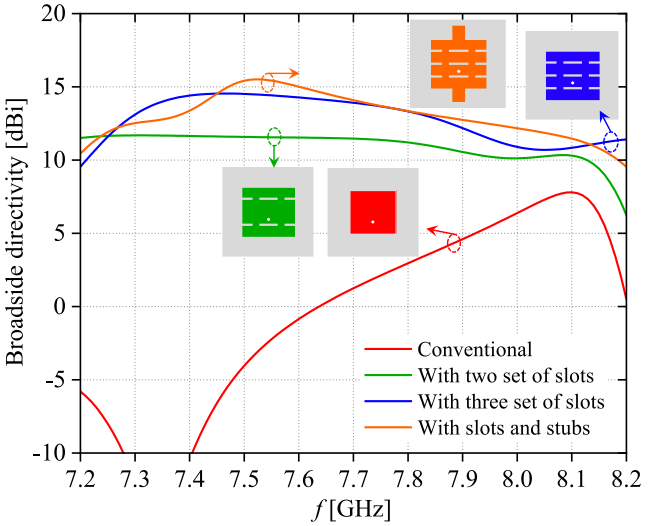

FIGURE 7. Directivity at broadside direction over the frequency of the four MPAs operating in the TM_{50}-like mode.

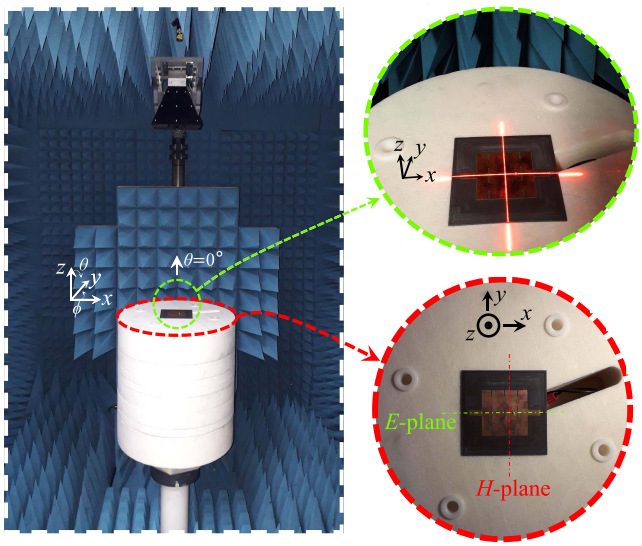

FIGURE 8. Measurement setup for the fabricated MPA with slots and stubs.

This figure concisely illustrates the evolution in directivity and radiation patterns of the MPAs. Fig. 5(a) depicts the radiation pattern behaviour in the *E*-plane at each design stage. For the conventional antenna (red), five radiation lobes are identified, with a *SLL* of 0 dB. With the introduction of two sets of slots (green), the pattern shifts to three radiation lobes, *SLL* improves to 1.8 dB, and directivity increases by 4.25 dB in the TM_{50}-like mode. The addition of a third set of slots (blue) maintains three lobes but significantly enhances *SLL* to 14.55 dB, with a 2.73 dBi directivity increase. Finally, incorporating slots and stubs (orange) maintains the three-lobe pattern with a slight *SLL* reduction to 19.0 dB and a further 0.82 dBi directivity improvement.

Fig. 5(b) shows the directivity radiation pattern behaviour in the *H*-plane for each MPA being compared. The conventional MPA (with results in red) displays three radiation lobes with a *SLL* of 6.3 dB, an unexpected outcome for a pure TM_{50}-like mode that can be attributed to the influence of higher-order modes at adjacent frequencies. With two sets of slots (green), the three-lobe pattern persists, but *SLL* significantly improves to 14.6 dB, and directivity in the maximum radiation direction increases by 4.25 dB from the conventional design. The introduction of a third set of slots (blue) maintains the three-lobe pattern, enhancing *SLL* further to 22.0 dB and directivity by an additional 2.73 dB. Incorporating slots and stubs (orange) also results in three radiation lobes, with *SLL* improvement to 15.8 dB and a 0.82 dB increase in maximum directivity over the prior configuration.

From previous analyses, it was evident that MPAs operating in the TM_{50}-like mode with three sets of slots, with and without stubs, yielded the most favorable performances. Consequently, Fig. 6 shows a comparative study between these configurations, in terms of the simulated reflection coefficient ($|S_{11}|$) and realized gain as a function of the frequency. For the antenna with three sets of slots (in blue), the impedance bandwidth (for $|S_{11}| < -10$ dB) is $Bw = 1.39\%$ (ranging from 7.502 to 7.607 GHz), while for the antenna with slots and stubs (in orange), it extends to $Bw = 1.84\%$ (from 7.485 to 7.624 GHz). Within the operating band, the antenna with three sets of slots (in dotted blue) achieves a maximum realized gain of 14.23 dBi (at 7.53 GHz), compared to the antenna with slots and stubs (in dotted orange), which reaches 15.09 dBi (at 7.55 GHz). Given these results, we opted to further investigate the MPA with slots and stubs as the primary radiator in this paper, detailing its manufacture and characterization subsequently.

IV. EXPERIMENTAL RESULTS AND DISCUSSION

A prototype of the proposed MPA was fabricated, as depicted in the inset of Fig. 8. It was fed by a single 50 Ω SMA coaxial probe. This prototype was produced using standard printed circuit board techniques on a machine running the

TABLE 3. Comparison with previous works of sidelobe-reduced and gain-enhanced higher order modes for patch antennas.

Reference	TM_{mn}-like mode	$(f_r)_{mn}$	Overall size*	G_0	D	Bw	A_{eff}	ε_{ap}	η
[8]	TM_{03}/TM_{05}	2.60	$0.011\lambda_0 \times 1.734\lambda_0 \times 1.734\lambda_0$	-	14.6	15.20	$2.303\lambda_0^2$	74.13	-
[9]	TM_{03}	4.20	$0.022\lambda_0 \times 1.541\lambda_0 \times 1.541\lambda_0$	12.8	13.36	1.53	$1.511\lambda_0^2$	63.97	88
[11]	TM_{05}	5.96	$0.040\lambda_0 \times 1.650\lambda_0 \times 1.650\lambda_0$	11.5	11.77	3.00	$1.107\lambda_0^2$	44.52	94
[12]	TM_{03}/TM_{05}	5.65	$0.014\lambda_0 \times 1.319\lambda_0 \times 1.319\lambda_0$	10.7	-	6.10	$0.923\lambda_0^2$	53.82	-
[13]	TM_{09}	12.52	$0.085\lambda_0 \times 2.920\lambda_0 \times 2.920\lambda_0$	15.5	15.96	2.70	$2.790\lambda_0^2$	33.10	90
[14]	TM_{03}	5.00	$0.033\lambda_0 \times 1.334\lambda_0 \times 1.334\lambda_0$	9.6	-	6.00	$0.723\lambda_0^2$	40.84	-
[15]	TM_{03}	5.80	$0.031\lambda_0 \times 1.306\lambda_0 \times 1.306\lambda_0$	10.5	10.77	8.50	$0.898\lambda_0^2$	52.45	94
[16]	TM_{10}/TM_{02}	3.30	$0.059\lambda_0 \times 0.924\lambda_0 \times 0.943\lambda_0$	9.1	9.83	12.65	$0.654\lambda_0^2$	74.64	85
[17]	TM_{30}	3.09	$0.015\lambda_0 \times 1.546\lambda_0 \times 1.443\lambda_0$	13.3	-	1.94	$1.699\lambda_0^2$	76.40	-
This work	TM_{50}	7.60	$0.040\lambda_0 \times 2.830\lambda_0 \times 2.830\lambda_0$	15.0	15.37	3.28	$2.494\lambda_0^2$	31.70	92

Resonance frequency (f_{mn}) in GHz; Maximum realized gain (G_0) in dBi; Directivity (D) in dBi; Bandwidth (Bw), Radiation (η) and aperture (ε_{ap}) efficiencies are given in percentage (%); Effective area (A_{eff}) in λ_0^2.
**Overall size ($h \times W \times L$) taken by ground plane physical dimensions in λ_0^3.*

Windows 11 operating system. The machine features a 12th Gen Intel Core i9 processor with 24 cores clocked at 3.2 GHz, and 128 GB of RAM. The electromagnetic properties of the antenna were evaluated in an anechoic chamber provided by Albatross Projects GmbH, using a Keysight FieldFox Vector Network Analyzer, model N995A, for the measurements.

A. BANDWIDTH

Fig. 9 presents both simulated and measured results for the reflection coefficient and maximum realized gain of the proposed microstrip patch antenna, demonstrating good concordance. The measured impedance bandwidth (Bw) spans from 7.49 to 7.74 GHz, equating to a bandwidth of 3.28%. The antenna's measured maximum realized gain was 15.0 dBi at 7.6 GHz, with a consistent performance exceeding 13 dBi throughout the entire useful bandwidth. We highlight that discrepancies between the simulated and measured results are primarily attributed to inaccuracies in the fabrication process.

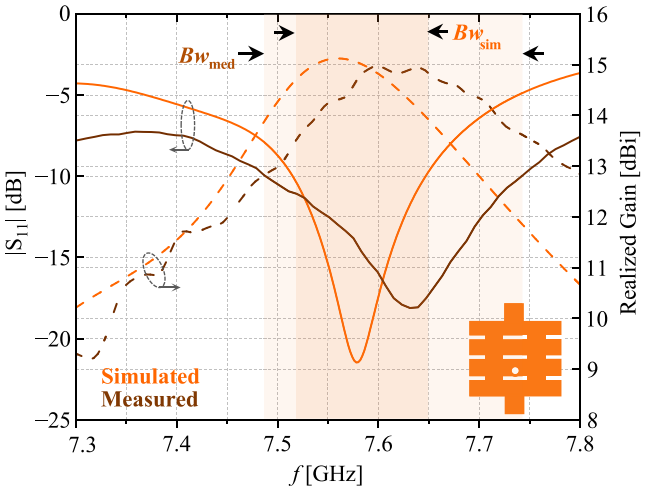

FIGURE 9. Simulated and measured results of the reflection coefficient and maximum realized gain of the proposed MPA.

B. RADIATION PERFORMANCE

Fig. 10 shows the simulated and measured radiation patterns of the proposed MPA at 7.6 GHz in both E- and H-planes, demonstrating good agreement between simulation and measurement. The main beams in the E-plane and H-plane are notably narrowed, with measured sidelobe levels in measurements reaching below −15.16 dB and −17.63 dB, respectively. Furthermore, analysis of the radiation patterns and maximum realized gain reveals that the proposed microstrip patch antenna achieves a radiation efficiency of 92%.

C. COMPARATIVE STUDY

A comparative analysis of the proposed MPA against other high-gain antenna designs is detailed in Table 3. This analysis includes operation mode, resonance frequency, overall size, maximum realized gain, directivity, percentage of impedance bandwidth, effective area, and radiation and aperture efficiencies, all based on measured results. The gain of the proposed MPA is only outperformed by the design in [13] by a margin of 0.5 dB. Nevertheless, our antenna boasts a smaller overall size and greater bandwidth than this model. Against high-gain patch antennas operating in TM_{50}-like or TM_{05}-like modes as reported in [8], [11], and [12], our design demonstrates superior gain across all compared models, achieving an improvement of at least 1 dB. Furthermore, our antenna secures a SLL of at least 15 dB.

V. CONCLUSION

In this paper, we propose a high-gain MPA operating in the TM_{50}-like mode, consisting of a square microstrip antenna with three sets of slots and two lateral stubs. A maximum realized gain of 15.0 dBi was measured at 7.6 GHz, despite the antenna's compact dimensions of only

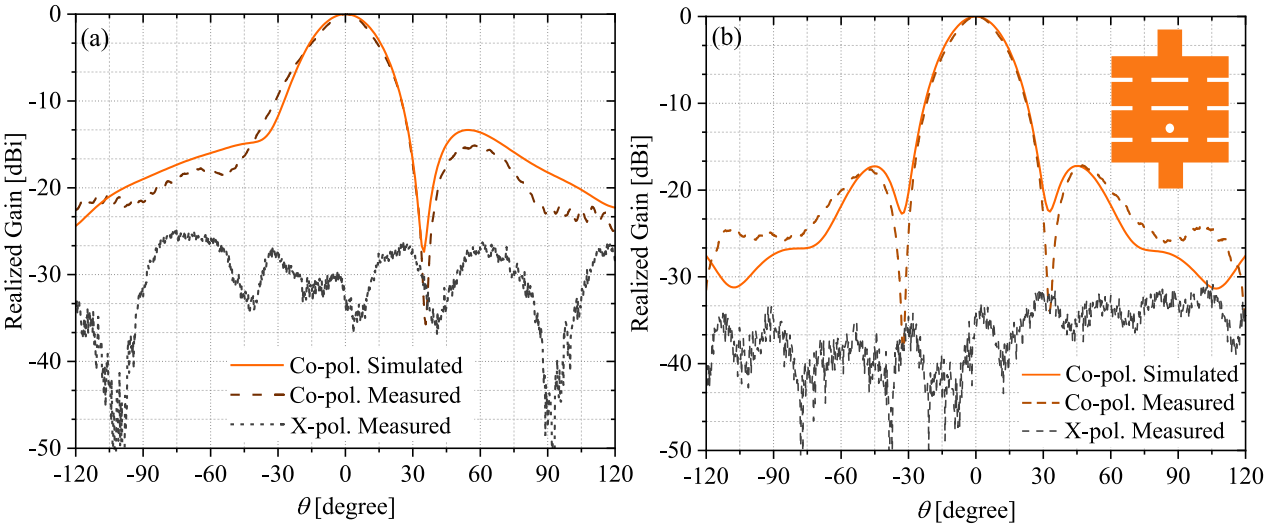

FIGURE 10. Simulated and measured radiation patterns of the proposed MPA. (a) *E*-plane. (b) *H*-plane.

$0.040\lambda_0 \times 2.830\lambda_0 \times 2.830\lambda_0$. The antenna also features low sidelobes, with an *SLL* better than 15 dB, and compared to other antennas reported in the literature, it offers an excellent gain-to-size ratio.

REFERENCES

[1] Z.-Y. Zhang, K. Lu, and K. W. Leung, "Gain enhancement of horn antenna using a metal lens," *IEEE Trans. Antennas Propag.*, vol. 71, no. 2, pp. 1337–1349, Feb. 2023.

[2] B. Feng, J. Lai, L. Li, C.-Y.-D. Sim, L. Deng, and X. Ding, "A dual-polarized shared-aperture antenna with conical radiation patterns and high gain for 5G millimeter-wave ceiling communications," *IEEE Trans. Antennas Propag.*, vol. 71, no. 3, pp. 2278–2289, Mar. 2023.

[3] J. Zhu, Y. Yang, Z. Hou, S. Liao, and Q. Xue, "Aperture-shared all-metal endfire high-gain parabolic antenna for millimeter-wave multibeam and sub-6-GHz communication applications," *IEEE Trans. Antennas Propag.*, vol. 71, no. 3, pp. 2784–2789, Mar. 2023.

[4] X.-C. Wang, Y.-J. Xia, J.-H. Yang, and W.-Z. Lu, "Wideband high-gain circularly polarized substrate integrated cavity antenna array for millimeter-wave applications," *IEEE Trans. Antennas Propag.*, vol. 71, no. 1, pp. 1041–1046, Jan. 2023.

[5] Y. Cheng and Y. Dong, "High-gain all-metal 3-D printed lens–horn antenna for millimeter-wave applications," *IEEE Antennas Wireless Propag. Lett.*, vol. 22, no. 2, pp. 308–312, Feb. 2023.

[6] Q. U. Khan, M. B. Ihsan, D. Fazal, F. M. Malik, S. A. Sheikh, and M. Salman, "Higher order modes: A solution for high gain, wide band patch antennas for different vehicular applications," *IEEE Trans. Veh. Technol.*, vol. 66, no. 5, pp. 3548–3554, May 2017.

[7] C. A. Balanis, *Antenna Theory: Analysis and Design*, 3rd ed. New York, NY, USA: Wiley, 2005.

[8] J. Anguera, A. Andújar, and J. Jayasinghe, "High-directivity microstrip patch antennas based on $TM_{odd\text{-}0}$ modes," *IEEE Antennas Wireless Propag. Lett.*, vol. 19, no. 1, pp. 39–43, Jan. 2020.

[9] X. Zhang, L. Zhu, and Q.-S. Wu, "Sidelobe-reduced and gain-enhanced square patch antennas with adjustable beamwidth under TM_{03} mode operation," *IEEE Trans. Antennas Propag.*, vol. 66, no. 4, pp. 1704–1713, Apr. 2018.

[10] W. Stutzman and G. Thiele, *Antenna Theory and Design*, 3rd ed. New York, NY, USA: Wiley, 2012.

[11] Y. He, Y. Li, W. Sun, Z. Zhang, and P.-Y. Chen, "Dual linearly polarized microstrip antenna using a slot-loaded TM_{50} mode," *IEEE Antennas Wireless Propag. Lett.*, vol. 17, no. 12, pp. 2344–2348, Dec. 2018.

[12] J. Wen, D. Xie, and L. Zhu, "Bandwidth-enhanced high-gain microstrip patch antenna under TM_{30} and TM_{50} dual-mode resonances," *IEEE Antennas Wireless Propag. Lett.*, vol. 18, no. 10, pp. 1976–1980, Oct. 2019.

[13] Y. He, Y. Li, W. Sun, and Z. Zhang, "Dual-Polarized, high-gain, and low-profile magnetic current array antenna," *IEEE Trans. Antennas Propag.*, vol. 67, no. 2, pp. 1312–1317, Feb. 2019.

[14] Y. Luo, Z. N. Chen, and K. Ma, "A single-layer dual-polarized differentially fed patch antenna with enhanced gain and bandwidth operating at dual compressed high-order modes using characteristic mode analysis," *IEEE Trans. Antennas Propag.*, vol. 68, no. 5, pp. 4082–4087, May 2020.

[15] A. Bhattacharyya, J. Pal, K. Patra, and B. Gupta, "Bandwidth-enhanced miniaturized patch antenna operating at higher order dual-mode resonance using modal analysis," *IEEE Antennas Wireless Propag. Lett.*, vol. 20, no. 2, pp. 274–278, Feb. 2021.

[16] J. Hao, N. Yan, Y. Luo, H. Fu, and K. Ma, "A low-cost dual-band multimode high-gain stacked-patch antenna based on SISL for 5G applications," *IEEE Antennas Wireless Propag. Lett.*, vol. 21, no. 1, pp. 4–8, Jan. 2022.

[17] Z. Ahmed, A. Muhammad, and M. B. Ihsan, "Improving the Sidelobe level, return loss and bandwidth of notch-loaded TM_{30} mode patch via fractal-slot," *IEEE Access*, vol. 10, pp. 19917–19924, 2022.

[18] J.-D. Zhang, L. Zhu, N.-W. Liu, and W. Wu, "Dual-band and dual-circularly polarized single-layer microstrip array based on multiresonant modes," *IEEE Trans. Antennas Propag.*, vol. 65, no. 3, pp. 1428–1433, Mar. 2017.

[19] R. W. Dearnley and A. R. F. Barel, "A comparison of models to determine the resonant frequencies of a rectangular microstrip antenna," *IEEE Trans. Antennas Propag.*, vol. 37, no. 1, pp. 114–118, Jan. 1989.

[20] Y. Zhang, W. Cao, Z. Qian, S. Shi, and W. Peng, "Low grating lobe array antenna with electrically large property based on TM_{50} mode," *IEEE Access*, vol. 7, pp. 32897–32906, 2019.

[21] *Ansys HFSS 2023*, Ansys Inc., Canonsburg, PA, USA, 2023.

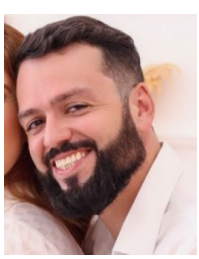

RENAN A. SANTOS received the M.Sc. degree in telecommunication engineering from the National Institute of Telecommunications (Inatel), Brazil, in 2016, and the Ph.D. degree in electrical engineering from the Federal University of Itajubá (Unifei), Brazil, in 2019. He has been a Professor of Electronic and Telecommunications Engineering with the Federal University of Uberlândia (UFU)-Patos de Minas Campus. His research focuses on electromagnetism applied to telecommunications (antennas, microwaves, and wave propagation).

HELTON S. BERNARDO was born in São Bernardo dos Campos, São Paulo, Brazil, in 1998. He received the B.Sc. degree in electrical engineering from the Federal Rural University of Pernambuco (UFRPE), Brazil, in 2022. He is currently pursuing the M.Sc. degree in electrical engineering with the School of Engineering, São Paulo State University (Unesp), São João da Boa Vista, Brazil. He works as research and perspective of study in the research line of devices antennas and circuits for radiofrequency-electronic telecommunication systems in millimeter waves. His interests for RF design antennas in millimeter waves for TM^{z}_{mn}-like modes operate in higher order, planar design of the RF device, and construction of the microstrip patches antennas for communications wireless systems.

DANILO H. SPADOTI received the degree in electrical engineering from the Federal University of Itajubá in 2002, and the master's degree in electrical engineering and the Doctorate degree in telecommunications from the USP—University of São Paulo in 2004 and 2008, respectively. In 2009, he was a Postdoctoral Research with the Nanophotonics Group, Cornell University, Ithaca, USA. In 2010, he was a Fapesp Postdoctoral Fellow with Universidade Presbiteriana Mackenzie. In 2012, he worked as a Visiting Researcher, with an Erasmus Mundus Scholarship, with the IMEC Research Center, Leuven, Belgium. He is currently an Associate Professor of Electrical Engineering with the Federal University of Itajubá, with an emphasis on telecommunications, working mainly on optical communications, photonic crystal optical fibers, and silicon photonics.

GUILHERME S. DA ROSA (Senior Member, IEEE) received the B.S. degree in electrical engineering from the Federal University of Santa Maria, Santa Maria, Brazil, in 2011, and the M.S. and Ph.D. degrees in electrical engineering from the Pontifical Catholic University of Rio de Janeiro, Rio de Janeiro, Brazil, in 2013 and 2017, respectively. He was a Professor with the Department of Electrical Engineering and the Center for Telecommunications Studies, Pontifical Catholic University of Rio de Janeiro from 2018 to 2024. In 2024, he joined São Paulo State University, São João da Boa Vista, Brazil, as a Professor with the School of Engineering. His current research interests include pseudo-analytical techniques for wave propagation modeling in complex media. He was a recipient of the Young Scientist Award from the URSI Commission B International Symposium on Electromagnetic Theory (EMTS) 2019, and the Young Scientist Award from the General Assembly and Scientific Symposium of the International Union of Radio Science (URSI-GASS) 2017.

RAFAEL A. PENCHEL (Member, IEEE) received the B.Sc. degree in telecommunications engineering from FUMEC University, Belo Horizonte, Brazil, in 2006, the M.Sc. degree in electrical engineering from the Federal University of Minas Gerais in 2009, and the Ph.D. degree in electrical engineering from the Pontifical Catholic University of Rio de Janeiro (PUC-Rio) in 2014. In 2015, he became a Postdoctoral Fellow with the National Institute of Telecommunications (Inatel). Since 2017, he has been a Professor with the Department of Electronic and Telecommunications Engineering, São Paulo State University (Unesp) and is part of the Center for Advanced and Sustainable Technologies Research Group. He has experience in electromagnetic theory with emphasis on microwave theory and antennas. His fields of research interest are passive devices and antennas for microwave and millimeter-wave frequency, mainly helical antennas, microstrip patch antennas, horn and reflector antennas; beamforming networks; and 3-D-printed antennas with complex geometries via plastic and metal additive manufacturing.